Bubble cloud generation by an airgun

Alexei Kouzoubov, Shane Wood

Defence Science and Technology Group, Adelaide, Australia

ABSTRACT

A previously developed model for the formation, dynamics and acoustic properties of a bubble cloud resulting from an underwater explosion is adapted for an airgun discharge. Improvements are made by taking into account the interaction between bubbles through water entrainment using an approximate solution. Model results are compared with the obtained experimental data and high-fidelity numerical simulations.

1. INTRODUCTION

A model representing the acoustic response from a bubble cloud generated by an underwater explosion (UNDEX), which has been insonified by an active sonar pulse, is of interest in a number of defence applications. For this, one needs to know the size distribution of the bubbles resulting from the disintegration of the initial explosion bubble. The bubble size distribution in the UNDEX remnant bubble cloud is not static and is changing with time, predominantly due to the rise of bubbles to the surface, but also with contributions due to bubble coalescence and break-up. The problem of the rising bubble cloud is mathematically simpler than the problem of the explosion bubble disintegration into smaller bubbles, but it is still too complex to solve it analytically. The complexity of the multiphase flow in a rising bubble cloud is caused by the presence of the bubbles of many different sizes and their interaction with each other, mainly through the water entrained by the bubble motion. A previously developed model (Kouzoubov, Castano et al. 2012) did not take into account the motion of entrained water and its influence on the bubble rise. However, it is obvious that the water entrained by the larger bubbles makes smaller bubbles rise faster, thus affecting the dynamics of the bubble size and spatial distribution and, therefore, the time history of its acoustic response. It is not simple to calculate the velocity of entrained water analytically even if the bubble size distribution in the cloud is known. Computational Fluid Dynamics (CFD) simulations of water entrainment by a rising bubble cloud are possible but with limited number of bubble size fractions. For a computationally efficient model it is important to develop a sufficiently accurate approximate model of a rising bubble cloud. Both experiments and high fidelity CFD simulations can help in the development and validation of such a model.

2. EXPERIMENTS

Experiments were conducted in the water tank of the Underwater Acoustic Scattering Laboratory (UASL) of the Defence Science and Technology (DST) Group. The following data were collected during the experiments: high-speed videos of the initial bubble, still images of the rising bubble cloud, velocity in the rising bubble cloud, acoustic scattering from and transmission through the bubble cloud. The set-up of the experiments, equipment used for data acquisition, and the obtained data will be described in this section.

2.1 Experiment set-up

The UASL water tank is of octagonal horizontal cross-section with major dimensions of 9 meters by 6 meters and depth of 4 meters. A charged airgun was placed in the tank at a depth of 2 meters. Various data were collected in a sequence of separate experiments; in other words, for every individual run only one type of data was obtained. High-speed videos and still camera images of the initial airgun bubble and the rising bubble cloud were obtained through a glass window in the tank wall. The velocity in the rising bubble cloud was measured using a Nortek Vectrino profiler with the sampling volume placed on the axis of the rising bubble cloud at 0.5 meters above the airgun. The acoustic scattering from the bubble cloud and acoustic transmission through it were obtained using the International Transducer Corporation (ITC) transducer with the centre frequency of 100 kHz. The transducer was positioned with its beam axis crossing the bubble cloud at 0.5 meters above the airgun. A hydrophone was placed on the transducer beam axis on the opposite side of the bubble cloud to measure the acoustic transmission through bubbles.

The airgun used in the experiments was manufactured by the Science Engineering Service (SES) of DST Group. The design was provided by Paul Brandner and Katrina de Graaf of the Australian Maritime College (AMC), who conducted research on the initial bubble dynamics and pressure field generated by the airgun. The design of the airgun is described in (de Graaf 2013) and was only slightly modified to fit the requirements of conducting experiments in the bigger tank of UASL. The volume of the airgun chamber is 14.5 mL.

2.2 Still Camera and High-speed Video Images

Still camera images of a rising bubble cloud, resulting from the airgun bubble break-up, have been obtained using a Nikon D4s digital SLR camera. An example of images sequence is shown in Figure 1, where every fourth image is shown. The initial pressure in the airgun was 6.89 MPa in this run. The frame rate is 11 frames per second. The exposure time is 1/8000 sec, the aperture is f2.8. A Zeiss prime lens Planar 1.4/85 ZF.2 with focal length of 85 mm was used. The images were taken in portrait orientation of the camera. Image size is 3280x4928.

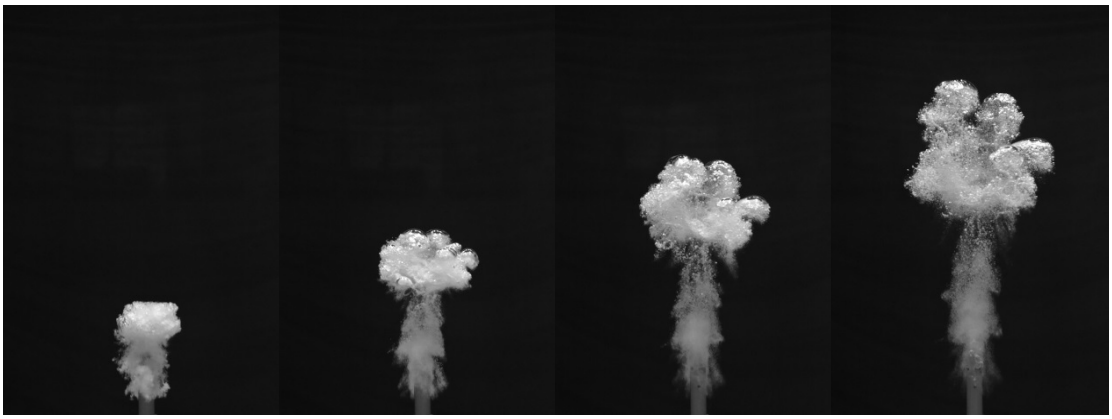

Figure 1. Sequence of still camera images of the rising bubble cloud from the airgun with an initial pressure of 6.89 MPa. The time interval between images is 4/11 s.

The image sequence gives some insight into the development of the bubble cloud. Initial airgun bubble is not the same as an explosion bubble. The explosion bubble is an almost perfect sphere filled with gas (Harris, Hyman et al. 2010), which then breaks into a cloud of small bubbles after three or four oscillations. The airgun bubble looks more like a foamy bubble. In other words, it is already a bubble cloud of very high volume fraction. Apparently, there is some distribution of bubbles in size, which, unfortunately, are impossible to measure at such a high volume fraction. One can see from the image sequence that there are very small bubbles, which stay in the vicinity of the airgun while larger bubbles in the cloud are quickly rising towards the water surface. It also can be noted that the coalescence of bubbles takes place, and very large bubbles can be seen at the top of the bubble cloud.

High-speed videos of the initial airgun bubble were obtained using a PCO1200hs camera. The full resolution of the camera is 1280x1024 pixels. The frame rate at full resolution is 500 fps but this can be increased by reducing the image resolution. In Figure 2, an example of two frames from a high-speed video of the initial bubble cloud is shown. The frame rate in this video was increased to 1000 fps by reducing the image resolution to 640x512 pixels. The initial pressure in the airgun was 6.89 MPa. The quality of images was improved by subtracting the background image, which was obtained by averaging several frames of the video before the air release. One can see from the images that the initial airgun bubble looks more like a bubble cloud with very high volume fraction, or like a foam bubble, which has four distinct lobes corresponding to the four gas release ports in the airgun.

Similar to the explosion bubble, the airgun bubble also undergoes several oscillations. By analysing the video frame-by-frame in Matlab and making measurements of the bubble diameter, the time history of the bubble diameter were obtained for several runs. Since the airgun bubble is not a perfect sphere, we measured the diameter of the horizontal cross-section of the bubble. The results are shown in Figure 3 for two different values of the initial air pressure in the airgun: 4.14 MPa and 6.89 MPa. Obviously the bubble at greater initial pressure grows to a larger size as can be seen from comparing the two plots. These results will be compared with the model prediction further in the report.

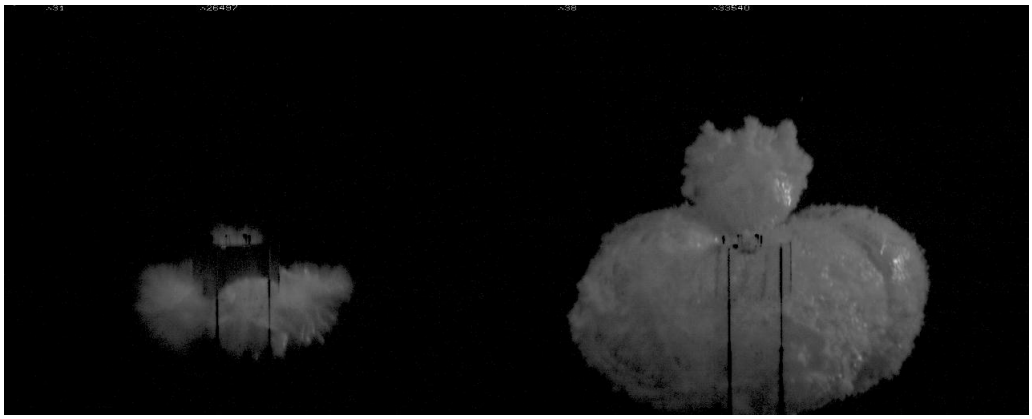

Figure 2. Example of frames of high-speed video of the initial airgun bubble. Time interval between frames is 7 ms.

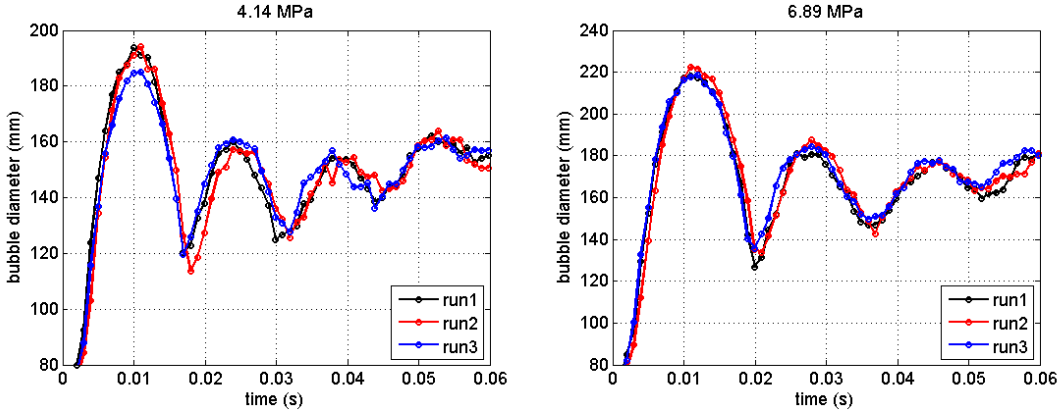

Figure 3. Time history of the airgun bubble diameter for different initial airgun pressures of 4.14 MPa (left plot) and 6.89 MPa (right plot).

2.3 Velocimetry data

It is of interest for further model development and validation to measure the velocity of the water entrained by a bubble cloud. It is, however, not straightforward to measure separately the velocity of entrained water and the velocity of the bubbles, especially in the multiphase flows of high volume fraction. In this experiment we used a Nortek Vectrino profiler, which is an acoustic Doppler velocimeter that has a four-beam probe to measure the three components of velocity over a range of 30 mm with a resolution of 1 mm and an output rate of up to 100 Hz. The maximum value of measured velocity is 3 m/s. The measurement technique requires the presence of some particles in the water to scatter sound back to the probe. Bubbles are good scatterers of sound, which makes an acoustic Doppler velocimeter a suitable instrument for measuring velocity in bubbly multiphase flows. This technique measures the velocity of the bubbles and not the velocity of entrained water, however we can assume that the velocity of bubbles will coincide with the velocity of water for very small bubbles. Thus, in the plume type flow with which we deal in this experiment, the probe is first passed by the large bubbles. The velocity measured in the first moments of the passing plume is the velocity of large bubbles and not that of water entrained by them. The large bubbles rise to the surface very quickly, followed by smaller bubbles in the plume, which are dragged upward with the water entrained by the larger bubbles. Thus, in the later stages of the plume the measured velocity will approach that of entrained water.

In this experiment the Vectrino profiler was placed horizontally with the sampling volume located approximately at the axis of the rising bubble cloud at the distance of 0.5 m above the airgun. The vertical component of the velocity is dominant in this flow. Its time history is shown for three runs in Figure 4 for the pressure of 6.89 MPa. The left plot shows data for individual runs, and the right plot displays the data averaged over those runs presented in the left plot.

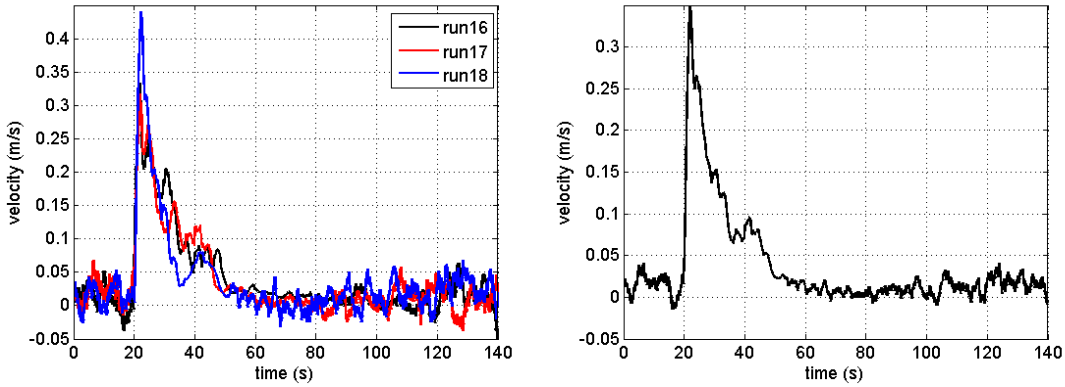

Figure 4. Vertical component of velocity in the bubble cloud at 0.5 m above the airgun with an initial pressure of 6.89 MPa. Left plot: Velocity data for three different runs; Right plot: velocity averaged over three runs.

2.4 Acoustic transmission and scattering

Measurements of the acoustic properties of the bubble cloud are important as they are related to the bubble size distribution in the cloud. The time history of acoustic transmission through the rising bubble cloud is shown in Figure 5 for an initial pressure of 6.89 MPa.

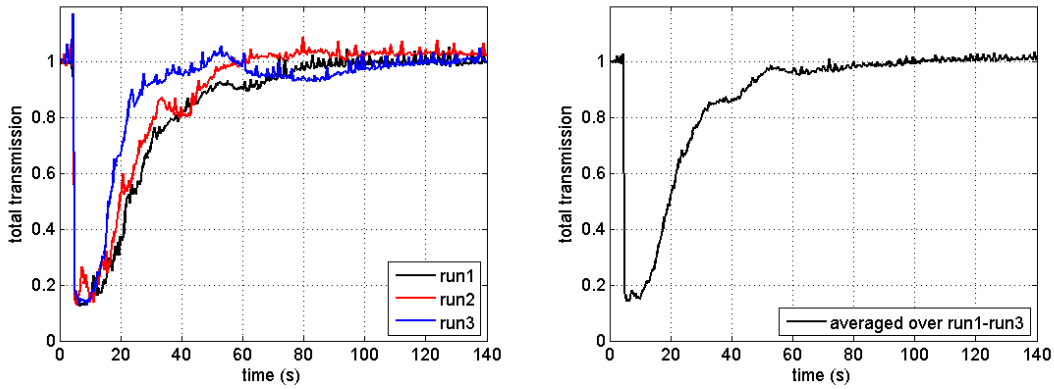

Figure 5. Time history of the total acoustic transmission through a rising bubble cloud at 0.5 m above the airgun with an initial pressure of 6.89 MPa. Left plot: three different runs; Right plot: average over three runs.

The line between the transmitter and the receiver passed through the axis of the bubble plume at 0.5 m above the airgun. The bubble cloud was insonified with short Linear Frequency Modulated (LFM) pulses emitted from a high-frequency transducer. A custom build ITC transducer with centre frequency of 100 kHz was used in these experiments. LFM pulse frequency range is from 20 to 240 kHz, with pulse duration of 770 μs. The sampling frequency was 5 MHz, the pulse repetition rate was 2.5 Hz. Both backscattered and transmitted through the bubble cloud signals were recorded.

3. MODELLING ASPECTS

Here we describe the improvements to the previously developed model of the UNDEX remnant bubble cloud (Kouzoubov, Castano et al. 2012) and apply it to the conditions of the laboratory experiments with an airgun. The model includes several parts: explosion globe dynamics, initial break-up of the explosion globe, turbulence created by the explosion globe fragmentation and further break-up of the bubbles by the turbulence. Previously, the time history of the bubble cloud properties was calculated under the assumption of the cloud being a collection of non-interacting bubbles. In this paper we improve the model of the rising bubble cloud dynamics by taking into account the interaction between bubbles via water entrainment.

3.1 Oscillation of initial bubble and its break-up into bubble cloud

The previously developed model of the UNDEX remnant bubble cloud (Kouzoubov, Castano et al. 2012) can be easily adapted to the airgun conditions. In the previous work, the oscillation of the initial explosion bubble is

based on the model described in (Geers and Hunter 2002) with the initial conditions of the explosion globe dynamics dependent on properties of the explosive material. For the airgun bubble, these initial conditions are described by the airgun volume and the initial air pressure. The results for the model of initial bubble oscillations are compared with the results of the tank experiments (Figure 6). The agreement between the model and experiment is not as good as in the case of the explosion globe oscillations (Kouzoubov, Castano et al. 2012), especially after first oscillation. The experimental data displays more damping of the oscillation. This is due to the difference between the explosion globe and the bubble formed by an airgun. The explosion globe is almost a perfect sphere, which breaks up into a cloud of smaller bubbles after three or four oscillations. The airgun bubble is not a bubble in strict terms but rather a foamy bubble, or a bubble cloud, which could be seen from Figure 2. This is mainly due to air discharge through relatively narrow ports, rather than expanding uniformly into ambient water. There are models developed specifically for an airgun bubble behaviour (de Graaf, Penesis et al. 2014, Li, Zhao et al. 2014), which may describe the airgun bubble oscillations more accurately. However, they use a number of empirical parameters, which have to be adjusted to match the measured data. The purpose of our research is not to develop a model of an airgun, but rather to test the model developed for the remnant bubble cloud resulting from an underwater explosion, keeping modification of the model to the minimum. It should be noted here that, due to the foamy nature of the airgun bubble, the initial bubble size distribution in the bubble cloud is estimated at the first minimum of the initial bubble oscillation and not at the third as in the case of explosion (Kouzoubov, Castano et al. 2012).

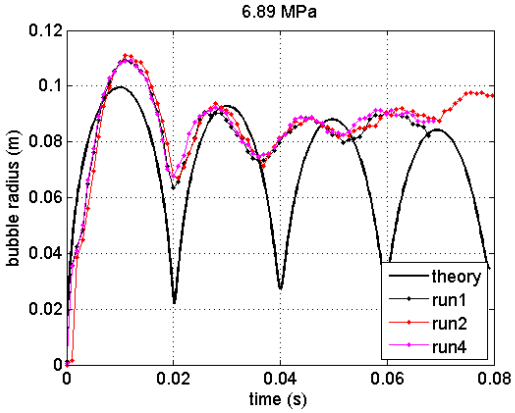

Figure 6. Comparison of the model of initial bubble oscillations with experiment.

Further elements of the model, such as bubbles further break-up by turbulence after initial bubble disintegration, do not require any modifications and are directly applied to the conditions of the tank experiment with the airgun. As a result, we obtain the initial and final bubble size distributions in the bubble cloud as shown in Figure 7.

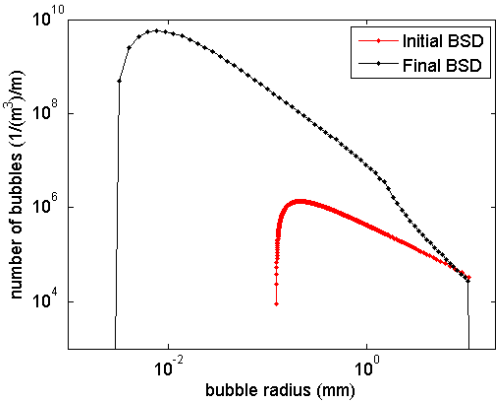

Figure 7. Initial and final bubble size distributions in the airgun experiment with an initial air pressure of 6.89 MPa.

3.2 Bubble cloud rise

Even in the relatively simple case of a cloud of uniform size bubbles, or monodisperse bubbles, it is not possible to find an exact analytical solution of the equations describing the velocities and volume fraction of the two phases: water and air. We will analyse this problem numerically using the commercial CFD package ANSYS CFX and will also try to find an approximate, but still numerical, solution. In this simplified model we assume that the flow is axisymmetric, the bubble cloud consists of monodisperse bubbles, and the bubbles in the cloud are rising at constant slip velocity defined by their size and assumed drag model. The influence of entrained water on the shape of the bubble cloud is described by a simple model. The equation of water velocity components, (u, v), in cylindrical coordinates, (r, z), are:

$$\frac{\partial u}{\partial z} + \frac{1}{r}\frac{\partial}{\partial r}(rv) = 0$$

$$\frac{\partial u}{\partial t} + u\frac{\partial u}{\partial z} + v\frac{\partial u}{\partial r} = \nu_w\left[\frac{\partial^2 u}{\partial z^2} + \frac{1}{r}\frac{\partial}{\partial r}\left(r\frac{\partial u}{\partial r}\right)\right] + \frac{M_D^{(z)}}{(1-\varphi_g)\rho_w} \tag{1}$$

$$\frac{\partial v}{\partial t} + u\frac{\partial v}{\partial z} + v\frac{\partial v}{\partial r} = \nu_w\left[\frac{\partial^2 v}{\partial z^2} + \frac{1}{r}\frac{\partial}{\partial r}\left(r\frac{\partial v}{\partial r}\right) - \frac{v}{r^2}\right] + \frac{M_D^{(r)}}{(1-\varphi_g)\rho_w}$$

In the above equations ν_w and ρ_w are the kinematic viscosity and the density of water, respectively, and the interfacial momentum transfer due to drag force has the form:

$$M_D^{(z)} = \frac{3}{4}\frac{C_D}{d_b}\varphi_g\rho_w U_s^2,\ M_D^{(r)} = 0 \tag{2}$$

where C_D and U_s are the drag coefficient and the slip velocity of the bubble of diameter d_b, respectively.

The gas volume fraction, φ_g, is assumed to remain constant inside the bubble cloud and is zero outside it. In the simplified model, the bubble cloud shape is approximated by an oblate spheroid. We assume that the initial shape of the bubble cloud is spherical.

During the rise of the bubble cloud, the water velocity at the bottom of the cloud, u_1, is obviously, higher than that at the top, u_2. This will lead to the gradual flattening of the spheroid. The vertical axis of the oblate spheroid, $2z_c$, can be estimated from the following equation:

$$z_c(t+\Delta t) = z_c(t) + \alpha(u_2 - u_1)\Delta t, \tag{3}$$

where $\alpha \le 0.5$. We also assume that the total volume of the bubble cloud remains constant, from which we find the horizontal semi-axis of the spheroid, r_c. Such an estimation of the shape of the bubble cloud can lead to excessive non-physical flattening, especially at high volume fractions. To overcome this without complicating the model, we set a minimum for the spheroid aspect ratio, $\varepsilon_c = z_c / r_c$. In our simulations, we usually assumed $\varepsilon_{c\min} = 1/8$. The speed of the bubble cloud rise is calculated as the sum of the bubble slip velocity, U_s, and the water velocity averaged over the vertical axis of the spheroid. To account for non-uniformity of the water velocity over the whole volume of the bubble cloud, we introduce some scaling factor $\beta < 1$:

$$U_c = U_s + \beta u_{cm}, \tag{4}$$

where:

$$u_{cm} = \frac{1}{2z_c} \int_{z_{ct}-z_c}^{z_{ct}+z_c} u(z, r=0) dz \,. \tag{5}$$

Here z_{ct} is the position of the centre of the spheroid calculated at each time step as $z_{ct}(t+\Delta t) = z_{ct}(t) + U_c \Delta t$.

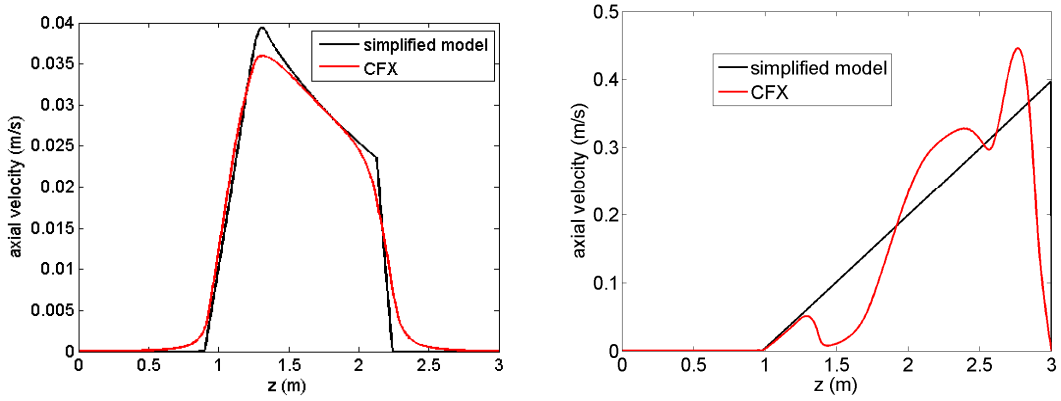

Figure 8. Axial velocity of water entrained by rising bubble cloud at 5 s. Left plot: bubble diameter is 9.68 mm, gas volume fraction is 0.00458; Right plot: bubble diameter is 62.5 mm, gas volume fraction is 0.29.

Figure 8 compares the simplified model of water entrainment by a rising cloud of monodisperse bubbles with corresponding numerical simulations using ANSYS CFX package. The plots show the velocity of entrained water at the vertical axis of the rising bubble cloud at 5 s from the start of the cloud rise. The results shown in the left plot of Figure 8 correspond to the case of low gas volume fraction of $4.58 \cdot 10^{-3}$ and relatively small bubble diameter of 9.68 mm. One can see a good agreement between the simplified model and high fidelity CFD simulations in this case. The agreement is not that good in the case of high gas volume fraction of 0.29 and large bubble diameter of 62.5 mm, results for which are shown in the right plot of Figure 8.

4. APPLICATION OF THE SIMPLIFIED MODEL TO THE AIRGUN BUBBLE CLOUD

In the above simplified model of water entrainment by a bubble cloud we assume that the bubble cloud consists of monodisperse bubbles. To apply this model to the rise of the airgun bubble cloud, where bubbles are distributed over quite a wide range of sizes (Figure 7), we make the following assumptions. We assume that all bubbles in the cloud are divided into 'large' and 'small' bubbles, where the 'Large' bubbles entrain water, and the 'small' bubbles are entrained by the water. We model the whole fraction of 'large' bubbles as a monodisperse fraction with an effective bubble size, for which we select the mean bubble diameter in the 'large' bubble fraction. To select the bubble size which divides the bubbles into 'large' and 'small' fraction, we analyse the bubble terminal velocity as a function of the bubble diameter. The terminal velocity is obtained from the balance of buoyancy and drag forces, in which the Grace Drag model is used (Clift, Grace et al. 1978). From this analysis we can derive that below a certain bubble diameter of about 2.7 mm the bubble velocity is decreasing sharply. We select this bubble size as the division between the 'large' and 'small' fractions.

In the case of the measured bubble size distribution in the airgun bubble cloud (Figure 7), the effective bubble size of 'large' bubbles in representative monodisperse fraction is 10.6 mm and its volume fraction is 0.287. Using these parameters in the simplified model of water entrainment by the bubble cloud, we will obtain the velocity field in the water column as a function of time and spatial coordinates. Comparison of the water velocity at the axis of the bubble cloud with the measurements is presented in Figure 9.

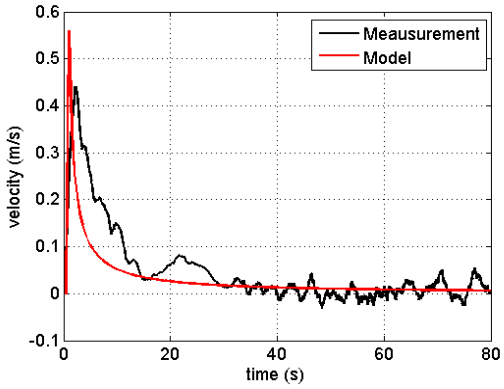

Figure 9. Comparison between the simplified model and measurements of the vertical component of velocity in the bubble cloud at 0.5 m above airgun.

One can see from the figure that simulated water velocity reaches approximately the same value as measured but drops much faster. There are two possible explanations for this. First, in the experiment there was some remnant leak of air from the airgun connecting hose, which, of course, is not taken into account in the model. This leak creates additional large bubbles for some time after the airgun discharge. Another reason for the slower drop of entrained water velocity in the model could be given as follows. Oscillations and break-up of the initial airgun bubble create many vortices in the water, which trap small bubbles. This slows down the rise of the bubbles. The vortices are not included into the model. Such an inclusion would be difficult even in CFD simulations unless they use the Large Eddy Simulation (LES) or the Direct Numerical Simulation (DNS) techniques, which are prohibitively time consuming even for this relatively simple geometry.

The next step in developing a model of the rising bubble cloud is to model the time history of the 'small' bubble fraction. We assume that small bubbles are initially uniformly distributed in a sphere of radius R_{c0} with the centre located at the final position, z_0, of the initial bubble before its break-up. The position of the centre, z_0 is the same as that of the bubble cloud of 'large' bubble fraction. The radius of the cloud of the 'small' bubble fraction could be, however, different from that of the cloud of 'large' bubble fraction: $R_{c0} = \alpha_s r_{c0}$, with $\alpha_s \geq 1$. For each bubble size and bubble initial position we find its rising trajectory by solving numerically the following kinematic equations:

$$\frac{dz_b}{dt} = U_s(d_b) + u(z,r,t), \qquad \frac{dr_b}{dt} = v(z,r,t) \tag{6}$$

with initial conditions:

$$z_b = z_{b0},\ r_b = r_{b0} \quad \text{at } t = 0 \tag{7}$$

Obviously, we assume in equation (6) that the velocity of a bubble relative to the water is equal to the bubble terminal velocity. We also neglect here the dependence of the terminal velocity on the bubble depth and calculate it at the initial bubble depth. From these bubble trajectories and the bubble size distribution in the initial bubble cloud, estimated from the model of bubble break-up, we can calculate the bubble size distribution at any point in the water and moment of time. For this, we first divide the initial bubble cloud into small volumes, $V_0 = \pi \Delta z_0 \left((r_{b0} + \Delta r_0)^2 - (r_{b0} - \Delta r_0)^2 \right)$. The number of bubbles of size d_b in the volume V_0 can be calculated as

$$n_{b0}(d_b, z_{b0}, r_{b0}) = \frac{n_b(d_b) V_0}{V_{bc}}, \tag{8}$$

where $V_{bc} = \frac{4\pi}{3} R_{c0}^3$ is the volume of the initial bubble cloud, and $(z_{b0} - z_0)^2 + r_{b0}^2 \le R_{c0}^2$. $n_b(d_b)$ is the total number of bubbles of size d_b in the initial bubble cloud after the bubble break-up by turbulence.

Once we know the bubble size distribution as a function of spatial coordinates and time, $n(d_b, z, r, t)$, we can calculate the acoustic transmission through the bubble cloud at a certain depth to compare it with the experiment. For this we need to calculate $n_p(d_b, r, t)$, the time history of the bubble size distribution per unit volume, averaged over the thickness Δz of a horizontal layer at height z_p above the airgun, at which the acoustic transmission through the bubble cloud was measured in the experiment. The absorption due to bubbles is calculated at the sound frequency , f , as (Medwin and Clay 1998)

$$\alpha_b(r,t,f) = 4.34 S_e = 4.34 \sum_{i=1}^{N} \sigma_e(d_{bi}, f) n_p(d_{bi}, r, t), \tag{9}$$

where S_e is the extinction cross section per unit volume, and σ_e is the extinction cross section of a single bubble. The corresponding equations are given in section 8.2 of (Medwin and Clay 1998) and we do not reproduce them here. Transmission through the bubble cloud can then be calculated as

$$\tau(t,f) = \frac{A_t}{A_0} = \exp\left(-\frac{2}{8.68} \int_0^{\infty} \alpha_b(r,t,f) dr \right), \tag{10}$$

where A_t and A_0 are the amplitude of the signal received by the hydrophone with and without the bubble cloud, respectively. To compare the simulated results, which are calculated at a single frequency value, to the measurements taken using frequency sweep pulse, we filter the transmitted signal into narrow frequency bands of 10 kHz using a 4-node Butterworth filter. The simulated results are then calculated at the centre frequency of each band. The comparison between simulated acoustic transmission through the rising bubble cloud with the measurement is presented in Figure 10 for one frequency band centred at 25 kHz, as most sensitive to the expected bubble size range. Here we also plot results obtained by the previous model where entrainment of the water was not taken into account. Although the model does not provide a perfect match with the experiment, the simulations using the simplified model of the water entrainment (black curves) compares better with the measurement after 20 s than the model of bubble rise in still water (blue curves).

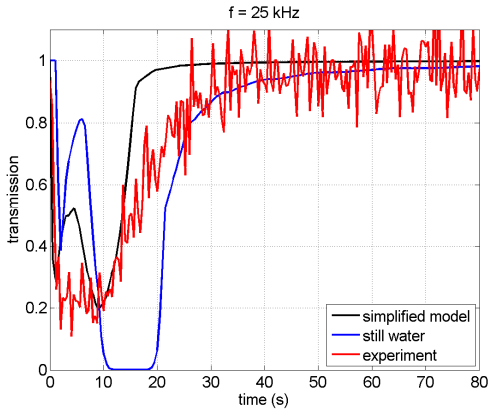

Figure 10. Time history of the acoustic transmission through the rising bubble cloud in a frequency band centered at 25 kHz.

5. CONCLUSIONS

A previously developed model of the remnant bubble cloud of underwater explosion has been improved by taking into account the interaction between bubbles through water entrainment. In the new model, the bubbles in a cloud are divided into two fractions of large and small bubbles and a simplified model of water entrainment by large bubble fraction has been developed. The dynamics of rising small bubbles is calculated using the assumption that their velocity is constant and is the sum of the terminal velocity in still water and that of the entrained water. The time history of the bubble size and spatial distribution in the cloud can then be easily computed. The calculation of acoustic properties of the bubble cloud is straightforward after that.

To validate the new model, an experiment was conducted in the acoustic tank of the Underwater Acoustic Scattering Laboratory. The underwater explosion was emulated by a small airgun. The explosion bubble dynamics model was modified for the airgun and demonstrated a fair agreement with the measured time history of the oscillating bubble radius for the first oscillation period, after which it was assumed that the initial bubble disintegrates into smaller bubbles. The simplified model of the water entrainment was validated by comparison of the water velocity at the axis of the bubble cloud with the corresponding measurements using an acoustic Doppler velocimeter. Finally, a comparison was made between the simulated and measured acoustic transmission through the bubble cloud. Although a perfect agreement was not achieved, an improvement against the previous model was demonstrated.

REFERENCES

Clift, R., J. R. Grace and M. E. Weber (1978). Bubbles, Drops, and Particles, Academic Press.

de Graaf, K. (2013). The Bubble Dynamics and Pressure Field Generated by a Seismic Airgun PhD, Australian Maritime College. University of Tasmania.

de Graaf, K. L., I. Penesis and P. A. Brandner (2014). "Modelling of seismic airgun bubble dynamics and pressure field using the Gilmore equation with additional damping factors." Ocean Engineering **76**: 32-39.

Geers, T. L. and K. S. Hunter (2002). "An integrated wave-effects model for an underwater explosion bubble." J. Acoust. Soc. Am. **111**(4): 1584-1601.

Harris, G., M. Hyman, J. Crane, G. Chahine, W. Lewis and J. Castano (2010). UNDEX Perturbation Test Program. Quick Look report. Naval Undersea Warfare Center. Newport.

Kouzoubov, A., J. Castano, C. Godoy and M. Hyman (2012). Acoustic Model of the Remnant Bubble Cloud from Underwater Explosion. Acoustics 2012. Fremantle, Australia.

Li, G. F., L. Zhao, W. Jianhua and C. Mingqiang (2014). "Air-gun signature modelling considering the influence of mechanical structure factors." Journal of Geophysics and Engineering **11**(2): 025005.

Medwin, H. and C. Clay (1998). Fundamentals of acoustical oceanography. Sydney, Academic Press.